View metadata, citation and similar papers at core.ac.uk
brought to you by CORE
provided by Okayama University Scientific Achievement Repository

Chemistry

Physical & Theoretical Chemistry fields

Okayama University *Year* 1996

Shape evolution of electrodeposited copper bumps with high peclet numbers

Kazuo Kondo
Okayama University

Keisuke Fukui
Himeji Institute of Technology

Mitsunori Yokoyama
University of Hokkaido

Kunio Shinohara
University of Hokkaido

This paper is posted at eScholarship@OUDIR : Okayama University Digital Information Repository.

http://escholarship.lib.okayama-u.ac.jp/physical_and_theoretical_chemistry/25

2. J. H. Nordlien, S. Ono, N. Masuko, and K. Nisancioglu, *This Journal*, **142**, 3320 (1995).
3. J. H. Nordlien, K. Nisancioglu, S. Ono, and N. Masuko, *Corros. Sci.*, In press.
4. J. H. Nordlien, K. Nisancioglu, S. Ono, and N. Masuko, *This Journal*, **143**, 2564 (1996).
5. O. Lunder, J. E. Lein, T. Kr. Aune, and K. Nisancioglu, *Corrosion*, **45**, 9, 741 (1989).
6. T. Beljoudi, C. Fiaud, and L. Robbiola, *ibid.*, **9**, 738 (1993).
7. O. Lunder, K. Nisancioglu, and R. S. Hansen, SAE Technical Paper No. 930755, SAE International, Warrendale, PA (1993).
8. O. Lunder and K. Nisancioglu, in *Progress in the Understanding and Prevention of Corrosion*, Vol. 2, J. M. Costa and A. D. Mercer, Editors, p. 1249, The Institute of Materials, London (1993).
9. *Standard Practice for Codification of Certain Nonferrous Metals and Alloys, Cast and Wrought*, B275, American Society for Testing of Materials, Philadelphia, PA (1980).
10. J. H. Nordlien, O. Lunder, H. Leth-Olsen, and K. Nisancioglu, *Extended Abstracts of the 47th Annual Meeting of the Scandinavian Society of Electron Microscopy*, T. Beisvåg, T.-H. Iversen, and J. K. Solberg, Editors, p. 111, SCANDEM 95, Trondheim, Norway (1995).
11. T. F. Malis and D. Steele, in *Ultramicrotomy for Materials Science in Workshop on Specimen Preparation for TEM Materials II*, R. Vol. 199, R. Andersen, Editor, Materials Research Symposium Proceedings, Materials Research Society, Pittsburgh, PA (1990).
12. R. Furneaux, G. E. Thompson, and G. C. Wood. *Corros. Sci.*, **18**, 853 (1978).
13. O. Lunder, T. Kr. Aune, and K. Nisancioglu, *Corrosion*, **43**, 291 (1987).
14. F. Mansfeld, S. Lin, S. Kim, and H. Shih, *ibid.*, **45**, 615 (1989).
15. B. R. W. Hinton, D. R. Arnott, and N. E. Ryan, *Mater. Forum*, **9**, 162 (1986).
16. N. A. Braaten, J. K. Grepstad, and S. Raaen, *Surf. Sci.*, **222**, 499 (1989); S. Raaen, N. A. Braaten, and J. K. Grepstad, *Phys. Scr.*, **41**, 1001 (1990).
17. N. A. Braaten and S. Raaen, *ibid.*, **43**, 430 (1991).

Shape Evolution of Electrodeposited Copper Bumps with High Peclet Numbers

Kazuo Kondo,[*,a,c] Keisuke Fukui,[b] Mitsunori Yokoyama,[a] and Kunio Shinohara[a]

[a]*Graduate School of Engineering, University of Hokkaido, Nishi-8, Kita-13, Sapporo 060, Japan*
[b]*Faculty of Engineering, Himeji Institute of Technology, Shosha, 2167, Himeji 671-22, Japan*

ABSTRACT

We report the shape evolution of initial copper bumps at Peclet numbers higher than a hundred. The role of vortices and of penetration flow within the cavity was discussed with numerical fluid dynamics computation to obtain a bump with a single hump at the center. The current distributions, or flux profiles, were calculated at the diffusion controlled overpotential and were compared with the electrodeposited bump shapes. For the 100 μm cavity width, the vortices increase at the upstream corners with Peclet numbers 1410 and 7311. The vortices are the local resistance of mass transfer to the cathode. These vortices cause the hollows in flux profiles at the upstream corner with these Peclet numbers. The penetration flow collides with the photoresist sidewall and the vortices decrease at downstream corners. These decreased vortices cause the increase in flux profile at downstream corners. For a 30 μm cavity width a single large vortex forms for the higher Peclet number 44,500 and a single hump in flux is achieved.

Introduction

Electrodeposited bumps are the indispensable microconnectors for high density interconnection in the latest microelectronics applications. For example, interconnection between microprocessors after 32 bits and random access memory (RAM) demand bumps, since the number of pads are several hundreds and the number is increasing for every new model. The bumps may be used not only as a substitute for wire bonding [tape automated bonding (TAB) and flip chip][1,2] but also as a new testing method for bare chips with high pin counts.[3] Another application is the interconnection between liquid crystal display (LCD) and driver chips, which are mostly interconnected with TAB. The bumps act as microconnectors of TAB technology and conduct digital signals from the chip to the LCD pixels.[4]

The bumps are electrodeposited onto dot-shaped cathodes several 10 to 200 μm in diameter. The cathode, or photolithographic patterns, are patterned by photomask and photoresist. The control of electrodeposited bump shapes as well as the uniformity in their heights are important for exhibiting proper interconnection reliability.[1] The bump shape with hump at the center, mushroom shape, is required for high density interconnection.

The role of mass transport in etching rectangular cavities formed by photoresist was discussed extensively by the following authors. Alkire and Deligianni developed a two-dimensional numerical fluid dynamics computation to study the electrolytic etching of copper.[5,6] The flow patterns were classified into two modes for the rectangular cavity of aspect ratios of 1.0 and 0.25, and their etch rate distributions were compared. Georgiadou and Alkire reported the experimental results on chemical etching of copper.[7,8] They also developed numerical fluid dynamics computation to study the presence of sparingly soluble surface film and compared the average etch rate with experiment for cavity aspect ratios of 1.0 and 0.20.[9] Shin and Economou studied electrolytic etching by numerical fluid dynamics of moving boundary for forced and natural convection.[10] They found that natural convection is effective for rinsing the dissolution products out of deep cavities. Jaw *et al.* studied jet electrochemical micromachining of throughholes. They found that changing nozzle diameter, cell voltage, nozzle-to-sample distance, and electrolyte flow is effective in shape control of throughholes.[11,12]

Bumping is electrodeposition onto dots and rectangular cavities formed by photoresist. Dukovic developed a two-dimensional numerical computation of tertiary current distribution. The moving boundary problem was discussed on shape evolution of copper electrodeposit and the effect of resist wall angle and leveling agent was reported.[13] Simon and Reichel developed a high speed gold bumping process and reported their bump shapes with a fountain-type plat-

* Electrochemical Society Active Member.
[c] Present address: Department of Applied Chemistry, Okayama University, 3-1-1 Tshima-Naka, Okayama 700, Japan.

ing cell.[14] Detailed studies on shape evolution of gold bumps were discussed by Kondo *et al.*[15] We studied the effects of dot diameter, electrolyte flow, and additive on bump shapes. The numerical fluid dynamics computation study on initial stage of gold and copper bumps at lower Peclet number of less than a hundred were also reported.[16,17]

The present investigation discusses the shape evolution of copper bumps at Peclet numbers higher than a hundred. The role of penetration and vortex flows within the cavities are discussed to obtain a bump with a single hump at the center which is necessary for high density interconnection. Further, the initial bump shapes electrodeposited at diffusion controlled overpotentials are compared with the current distribution calculated by the numerical fluid dynamics.

Numerical Analysis and Experimental

Two-dimensional cross sections of dot patterns were analyzed numerically by solving the equation of continuity, Navier-Stokes equations, and mass-transfer equation. The computational area and the boundary conditions are illustrated in Fig. 1 and the details are given in Ref. 17. The numerical method proposed by Patankar[19] is adopted for discretization and pressure equation calculation. The dimensionless Peclet number is defined as follows

$$\mathrm{Pe} = hu_{y=2h}/D$$

Electrodeposition and photolithography conditions are presented in Ref. 17. The photolithographed substrates have dot patterns of 100 μm in diam and these patterns are located 8 mm from the center of the rotating disk electrode. The substrates were attached to the rotating disk electrode and rotational speed varied from 200 to 3000 rpm. The bumps were electrodeposited potentiostatically at the diffusion controlled overpotential. The bumps were observed by scanning electron microscopy (SEM) with sample stage tilting of 1.22 rad.

Results and Discussion

Stream functions and isoconcentration contours.— Figure 2 shows the normalized stream functions for the 100 μm cavity width calculated by the numerical fluid dynamics. Cathodes are located at the cavity bottom and are illustrated with slant lines. Photoresists 10 μm in height are located at both sides of the cathodes. The electrolyte flows from left to right as indicated by arrows. The Peclet numbers are 126, 1410, and 7311 for Fig. 2 a, b, and c, respectively.

The vortices occur at the corners of cathodes both at up- and downstream. The streamline 6 is the penetration flow which starts from the upstream side bulk solution to the cathode centers at cavity bottoms and to the downstream side bulk solution. The vortices at upstream side corners increase and grow toward the downstream side with the increase in Peclet numbers. The vortices at the downstream side corners decrease with the increase in the Peclet numbers.

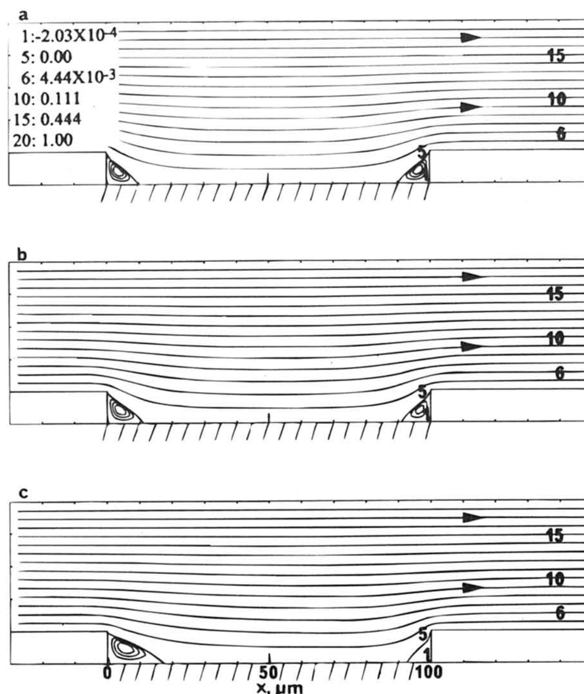

Fig. 2. Effect of Peclet numbers on stream lines. The cavity width was 100 μm. (a) Pe = 126, (b) Pe = 1410, and (c) Pe = 7311.

Figure 3 shows the isoconcentration contours for the 100 μm cavity width calculated by numerical fluid dynamics. The location of cathodes and photoresists are the same as in Fig. 2. The copper ions are consumed on cathodes at the cavity bottoms and the concentration boundary layer develops. The Peclet numbers are 126, 1410, and 7311 for Fig. 3a, b, and c, respectively. The iso-

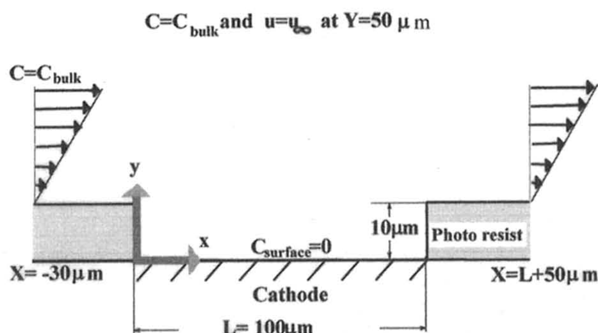

Fig. 1. Illustration of two-dimensional cross section of photoresist and cathode; x- and y-coordinates and the boundary conditions are shown.

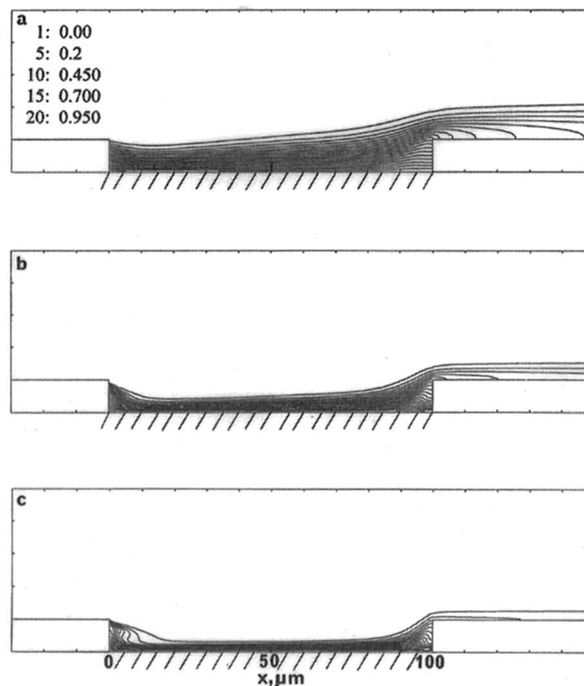

Fig. 3. Effect of Peclet numbers on isoconcentration contours. The cavity width was 100 μm. (a) Pe = 126, (b) Pe = 1410, and (c) Pe = 7311.

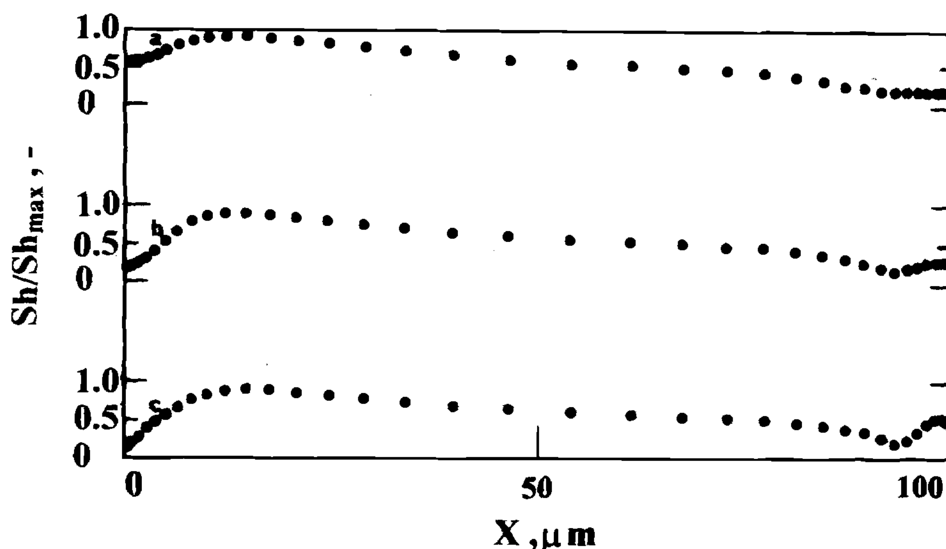

Fig. 4. Effect of Peclet numbers on flux (normalized Sherwood number) profiles. The cavity width was 100 μm. (a) Pe = 126, (b) Pe = 1410, and (c) Pe = 7311.

concentration contours converge and come close to the cathodes with the increase in the Peclet numbers. The isoconcentration contours form distortions both at up- and downstream corners for Fig. 3b and c because of the large convection within the vortices.

Flux profiles on cathodes.—Figure 4 shows the current distributions, or flux profiles, for the 100 μm cavity width calculated from the isoconcentration contours. The flux is expressed by the ratio of local and maximum dimensionless Sherwood numbers, Sh/Sh_{max}. The Peclet numbers are 126, 1410, and 7311 for Fig. 4a, b, and c, respectively. For the Peclet number of 126, Fig. 4a, the Sh/Sh_{max} is constant at the upstream side of $x = 0$ to 10 μm. This ratio decreases toward the downstream and also becomes constant at the downstream side of $x = 90$ to 100 μm. For Peclet number 1410 (Fig. 4b), the ratio is low at $x = 0$ and increases rapidly from $x = 0$ to 10 μm. The ratio decreases toward the downstream side and slightly increases again at the downstream side of $x = 90$ to 100 μm. For Peclet number 7311 (Fig. 4c), the ratio is also low at $x = 0$ and increases rapidly from $x = 0$ to 10 μm. The ratio decreases toward the downstream side and increases at the downstream side of $x = 95$ μm.

At the upstream side corner, the vortices increase and grow toward the downstream side with the increase in Peclet numbers (Fig. 2). The vortices are the resistance of mass transfer to the cathode because the vortices recirculate within themselves and are not able to capture the copper ion.[16,17] These resistances of mass transfer flatten the flux profile at the upstream side corner for Peclet number 126 (Fig. 4a). Further increase in the Peclet numbers to 1410 and 7311 decrease the flux and cause hollows in the flux profiles at upstream side corners (Fig. 4b, c). At the center of the cavity, the flux decreases gradually from the up- to the downstream side because of the penetration flows (Fig. 2). These penetration flows transport fresh bulk electrolyte of high copper ion concentration from the upstream side to the bottom surface and to the downstream side. As this bulk electrolyte moves from the up- to the downstream side along the cathode surface, the copper ions are consumed and the flux decreases. At the downstream side corners, the vortices decrease with an increase in the Peclet numbers of 1410 and 7311 (Fig. 2b, c). These increase the flux at the downstream side corners (Fig. 4b, c). These decreases in vortices are due to the collision between the penetration flows and the photoresist sidewalls at the downstream side corners.

Bump shape evolution at diffusion controlled overpotential.—Figure 5 shows the cathodic polarization curves for Peclet numbers 126, 498, and 1410. The current density increases as the Peclet numbers increase. The potential of −450 mV *vs.* 3.33 mol KCl-AgCl is diffusion control for all Peclet numbers and this potential is used to electrodeposit the bumps.

Figure 6 shows SEM micrographs of initial bump shapes electrodeposited on the dot cathode 100 μm in diameter at the potential −450 mV *vs.* 3.33 mol KCl-AgCl. Total number of coulombs was 4.0 C/cm^2. The larger arrow in Fig. 6a shows the direction of electrolyte flow. The bump shape is flat at the upstream side corner and this is indicated with a smaller arrow in Fig. 6a. The bump height decreases toward the downstream and also becomes flat at the downstream side corner. For Fig. 6b, the bump height increases rapidly at the upstream side corner and the height decreases toward the downstream side and slightly increases again at the downstream side corner. For Fig. 6c, the bump height also increases rapidly at the upstream side corner and the height decreases toward the downstream side and increases again at the downstream side corner (indicated with an arrow). These observed initial bump shapes coincide well with the calculated flux profile shown in Fig. 4.

Shape evolution at higher Peclet numbers.—The two vortices exist separately at the up- and downstream side corners for 100 μm cavity width (Fig. 2). These vortices are

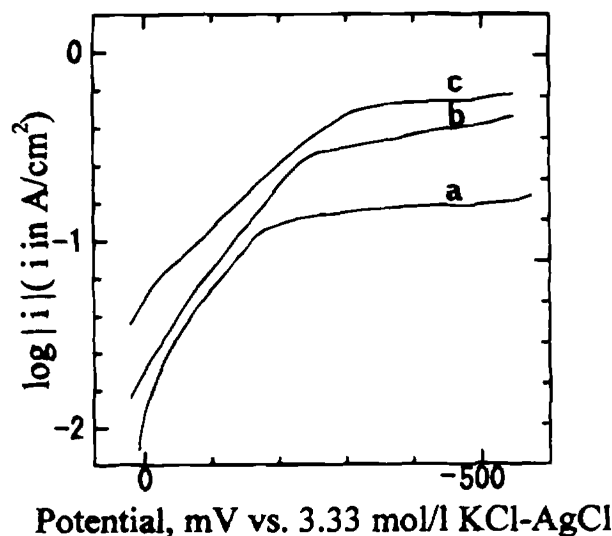

Fig. 5. Cathodic polarization curves. (a) Pe = 126, (b) Pe = 498, and (c) Pe = 1410.

Fig. 6. Effect of Peclet numbers on bump shapes for 100 μm dot diameter. The bumps were formed by potentiostatic electrolysis at the diffusion controlled region of −450 mV *vs.* 3.33 mol KCl-AgCl. (a) Pe = 126, (b) Pe = 1410, and (c) Pe = 7311.

expected to merge into one for shorter cavity width at higher Peclet numbers. Numerical fluid dynamics results are shown below.

Figure 7 shows the stream functions and the isoconcentration contours. For the Peclet number of 7311, the two vortices grow toward the center and start to merge togeth-

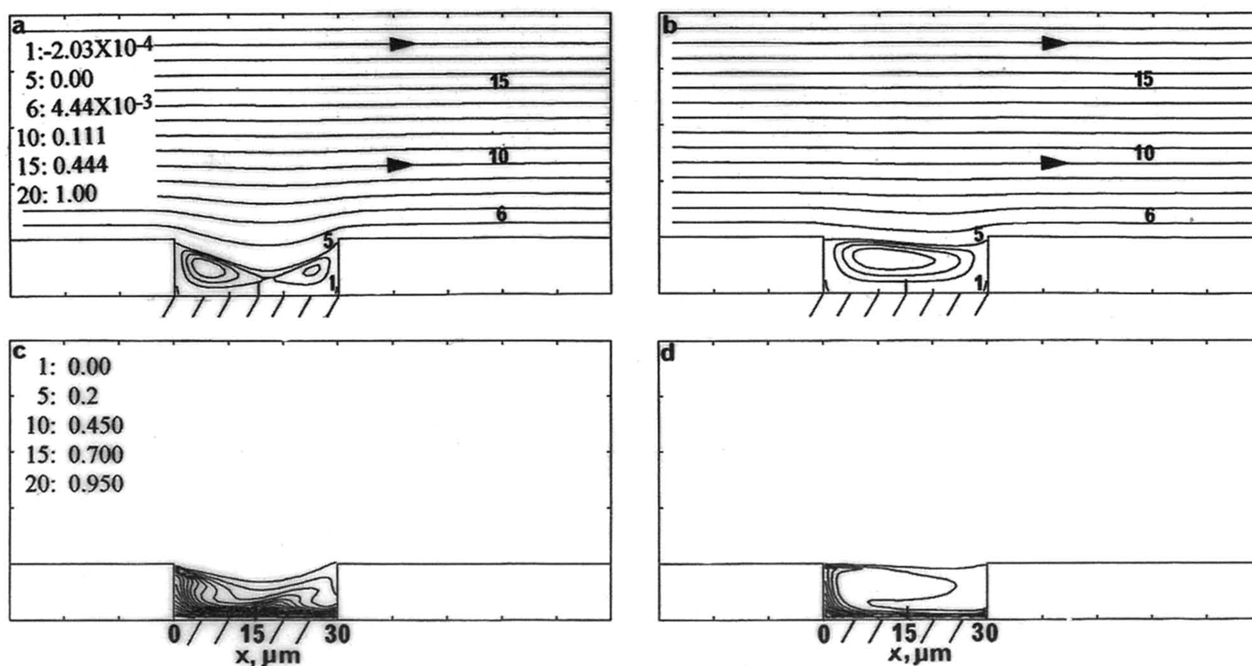

Fig. 7. Effect of Peclet numbers on stream lines and isoconcentration contours. The cavity width was 30 μm. Stream lines for (a) Pe = 7311 and (b) Pe = 44,500; isoconcentration contours for (c) Pe = 7311 and (d) Pe = 44,500.

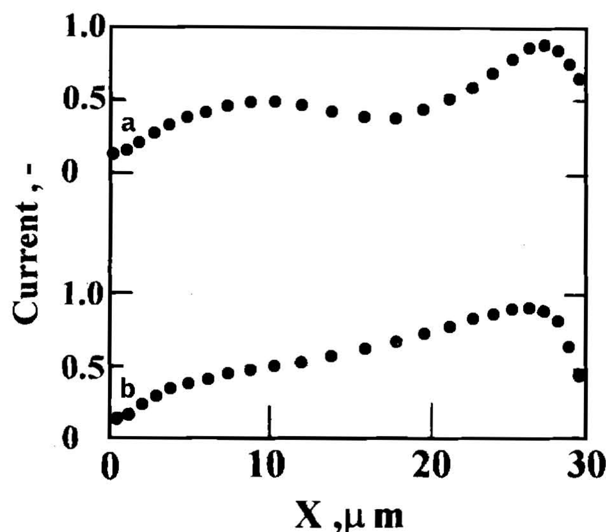

Fig. 8. Effect of Peclet numbers on flux (normalized Sherwood number) profiles. The cavity width was 30 μm. (a) Pe = 7311 and (b) Pe = 44,500.

er at x = 18 μm. For Peclet number 44,500, two vortices merge into one and form a single large vortex. The isoconcentration contours form distortions because of the large convection within the vortices. The vortices circulate clockwise (Fig. 2, 7). Flow direction of these vortices along the cathode surface are from the down- to the upstream side. Because of this flow direction, the copper ions are consumed and the flux decreases toward the down- to upstream side.

Figure 8 shows the flux profiles on cathodes. Figure 8a has two peaks in its profile which correspond to the existence of two vortices. One peak is at x = 10 μm at the upstream side and the other peak is at x = 28 μm at the downstream side. In Fig. 8b, single hump at x = 25 μm exists which corresponds to the formation of a single large vortex at the cavity center.

Conclusion

The current distributions, or flux profiles, were calculated by the numerical fluid dynamics and compared with the initial bumps electrodeposited at Peclet numbers higher than a hundred. The role of penetration and vortex flows within the cavities were discussed in order to obtain bumps with single humps at the centers.

1. The vortices form separately both at up- and downstream side corners for 100 μm cavity width. These vortices, however, merge into one and form a single large vortex for the 30 μm cavity width of high Peclet number 44,500.

2. For the 100 μm cavity width of Peclet number 126, the current distribution, or the flux profile, is constant at the upstream side corner. The flux profile decreases toward the downstream and also becomes constant at the downstream side corners. For Peclet number 1410, the flux decreases and increases rapidly at the upstream side corner and increases slightly at the downstream side corner. For Peclet number 7311, the flux increases significantly at the downstream side. These flux profiles coincide well with the initial bump shapes electrodeposited on the 100 μm diameter patterns at the diffusion controlled overpotential.

For the 30 μm cavity width of the Peclet number of 44,500, however, the flux profile has a single hump at the center.

3. The vortices are the resistance of mass transfer to the cathode. The vortices increase with the increase of the Peclet numbers 1410 and 7311 at the upstream side corner. These vortices decrease in flux profile at the upstream side corners. The vortices decrease with the increase of the Peclet numbers at the downstream side corner. This decrease in vortices causes an increase in flux profiles.

For the 30 μm cavity width of Peclet number 7311, the two vortices at the up- and downstream side start to merge together. For Peclet number 44,500, the vortices merge into one and form a single large vortex. The flux profile of the single hump at the center is achieved because of this single large vortex.

Acknowledgment

The authors thank Professor R. C. Alkire and his research group for instructive discussions. This work was supported by TEPCO Research Foundation.

Manuscript submitted May 20, 1996; revised manuscript received Oct. 10, 1996.

Hokkaido University assisted in meeting the publication costs of this article.

LIST OF SYMBOLS

c	concentration, mol m^{-3}
D	diffusion coefficient, m^2 s^{-1}
h	resist height, m
k	$[(D\, \partial c/\partial y\|_{y=0})/\Delta c]$ mass transfer coefficient, m s^{-1}
L	cathode length, m
P	static pressure, Pa
Pe	Peclet number, Pe = $hu_{y=2h}/D$
r	radius of photomask pattern, m
Sh	Sherwood number, Sh = kL/D
Sh_{max}	maximum value of the Sherwood number
u	velocity in the x-direction, m s^{-1}
v	velocity in y-direction, m s^{-1}
x	coordinate in the streamwise direction, m
y	coordinate normal to the cathode surface, m
ν	kinematics viscosity, m^2 s^{-1}
μ	viscosity, kg m^{-1} s^{-1}
ρ	density, kg m^{-3}
Ω	number of rotation, s^{-1}

REFERENCES

1. R. R. Tummala and E. J. Rymaszewski, *Microelectronics Packaging Handbook*, p. 361, Van Nostrand Reinhold, New York (1989).
2. M. Sage and D. Gross, *Hardware Developments in Electronic Systems*, BPA (Technology & Management) Ltd., Surrey, England (1992).
3. Y. Yamamoto, M. Sugimoto, and K. Miyake, in *Proceedings of ISHM '93*, p. 370, Dallas, TX (1993).
4. K. Hatada, *Introduction to TAB Technology* (in Japanese), Kougiyouchiyousakai, Tokyo (1989).
5. R. C. Alkire and H. Deligianni, *This Journal*, **135**, 1093 (1988).
6. R. C. Alkire, H. Deligianni, and J-B Ju, *ibid.*, **137**, 818 (1990).
7. M. Georgiadou and R. C. Alkire, *ibid.*, **140**, 1340 (1993).
8. M. Georgiadou and R. C. Alkire, *ibid.*, **140**, 1348 (1993).
9. M. Georgiadou and R. C. Alkire, *ibid.*, **141**, 679 (1994).
10. C. B. Shin and D. J. Economou, *ibid.*, **138**, 527 (1991).
11. S.-J. Jaw, J. M. Fenton, and M. Datta, in *Electrochemical Microfabrication II*, M. Datta, K. Sheppard, and J. O. Dukovic, Editors, PV 94-32, p. 217, The Electrochemical Society Proceedings Series, Pennington, NJ (1994).
12. S.-J. Jaw, J. M. Fenton, and M. Datta, in *High Rate Metal Dissolution Process*, M. Datta, B. R. MacDougall, and J. M. Fenton, Editors, PV 95-19, p. 236, The Electrochemical Society Proceedings Series, Pennington, NJ (1995).
13. J. O. Dukovic, *IBM J. Res. Develop.*, **37**, 125 (1993).
14. J. Simon and H. Reichel, in *Proceedings of the 9th International Microelectronics Conference*, p. 265, Ohmiya, Japan (1996).
15. K. Kondo, T. Miyazaki, and Y. Tamura, *This Journal*, **141**, 1644 (1994).
16. K. Kondo and K. Fukui, *Kagaku-kougaku Ronbunshu*, **22** (1996).
17. K. Kondo, K. Fukui, K. Uno, and K. Shinohara, *This Journal*, **144**, 1880 (1996).
18. H. Schlichting, *Boundary Layer Theory*, p. 93, McGraw-Hill, New York (1968).
19. S. V. Patankar, *Numerical Heat Transfer and Fluid Flow*, Hemisphere Publishing Corp., New York (1980).